Available online at www.sciencedirect.com
ScienceDirect
Journal of Power Sources 169 (2007) 17–24
JOURNAL OF POWER SOURCES
www.elsevier.com/locate/jpowsour

In situ high temperature neutron powder diffraction study of $La_2Ni_{0.6}Cu_{0.4}O_{4+\delta}$ in air: Correlation with the electrical behaviour☆

A. Aguadero[a,*], J.A. Alonso[b], M.T. Fernández-Díaz[c], M.J. Escudero[a], L. Daza[a,d]

[a] *Centro de Investigaciones Energéticas Mediambientales y Tecnológicas (CIEMAT), Av. Complutense 22, 28040 Madrid, Spain*
[b] *Instituto de Ciencia de Materiales de Madrid (CSIC), Cantoblanco, 28049 Madrid, Spain*
[c] *Institute Laue-Langevin (ILL) 156X, F-38042 Grenoble Cedex 9, France*
[d] *Instituto de Catálisis y Petroleoquímica (CSIC), Marie-Curie 2, Campus Cantoblanco, 28049 Madrid, Spain*

Available online 6 February 2007

Abstract

The knowledge of the thermal evolution of the crystal structure of a cathode material across the usual working conditions in solid oxide fuel cells is essential to understand not only its transport properties but also its chemical and mechanical stability in the working environment. In this regard, high-resolution neutron powder diffraction (NPD) measurements have been performed in air from 25 to 900 °C on O_2-treated (350 °C/200 bar) $La_2Ni_{0.6}Cu_{0.4}O_{4+\delta}$. The crystal structure was Rietveld-refined in the tetragonal *F*4/*mmm* space group along all the temperature range. The structural data have been correlated with the transport properties of this layered perovskite. The electrical conductivity of O_2-treated $La_2Ni_{0.6}Cu_{0.4}O_{4+\delta}$ exhibits a metal (high T)-to-semiconductor (low T) transition as a function of temperature, displaying a maximum value of 110 S cm^{-1} at around 450 °C. The largest conductivity corresponds, microscopically, to the shortest axial Ni–O2 distance (2.29(1) Å), revealing a major anisotropic component for the electronic transport. We have also performed a durability test at 750 °C for 560 h obtaining a very stable value for the electrical conductivity of 87 S cm^{-1}. The thermal expansion coefficient was 12.8×10^{-6} K^{-1} very close to that of the usual SOFC electrolytes. These results exhibit $La_2Ni_{0.6}Cu_{0.4}O_{4+\delta}$ as a possible alternative cathode for IT-SOFC.

Keywords: *In situ* structural evolution; Neutron powder diffraction; IT-SOFC; Cathode; K_2NiF_4; Metal–insulator transition

1. Introduction

One of the most important handicaps for the commercialization of solid oxide fuel cells (SOFC) is their high operating temperatures (900–1000 °C). Nowadays, the efforts in this area are focused on reducing the operating temperature without decreasing the cell efficiency. For these purpose, 'mixed ionic electronic conductors' (MIEC) appear to be some of the most promising cathode materials [1,2] due to the improvement of the kinetic of the cathode reaction by replacing the triple phase boundary zone (cathode-electrolyte-air) to a double inter-phase (cathode-air) at low temperatures (650–850 °C). In this case, MIEC materials provide not only the electrons for the reduction of oxygen but also the ionic conduction required to ensure the transport of the formed oxygen ions between the double inter-phase and the electrolyte.

Materials with K_2NiF_4 structure, have received considerable attention as novel cathodes for intermediate temperature SOFC's due to its interesting transport properties [3–5]. The crystal structure of these phases can be described as a staking of perovskite layers alternating with rock salt layers along the *c* direction [6]. The oxygen transport occurs via a complex mechanism combining interstitial migrations in the rock salt layers and vacancy migration in the perovskite planes [7,8]. The contribution of the interstitial mechanism appears to be more important than the vacancy migration mechanism, since higher oxygen contents can be achieved in these compounds, usually with a positive effect on their ionic conductivity [9,10]. In this way, treatments under high oxygen pressure on K_2NiF_4 materials appears to be a promising method to improve the transport properties of this compounds by means of incorporating interstitial oxygen into the crystal lattice and by increasing the ionic mobility of the oxygen atoms [11].

☆ This paper is presented at the 2nd National Congress on Fuel Cells, CONAPPICE 2006.

* Corresponding author.
E-mail address: ainara.aguadero@ciemat.es (A. Aguadero).

0378-7753/$ – see front matter © 2007 Published by Elsevier B.V.
doi:10.1016/j.jpowsour.2007.01.075

Several investigations have been directed to determine the crystal structure of $La_2NiO_{4+\delta}$ as a function of the oxygen stoichiometry [12,13]. Some neutron diffraction studies have been carried out either at RT (room temperature) [14,15] or at high temperature under vacuum [16,17]. We have performed, for the first time, a study of the thermal evolution of the crystal structure of $La_2NiO_{4,30}$ in air, founding very interesting relations between the structural evolution, the electrical behaviour and the oxygen content of this material [18].

The electrical conductivity of $La_2Ni_{0.6}Cu_{0.4}O_{4+\delta}$ is slightly bigger than the conductivity of $La_2NiO_{4+\delta}$ [11]. This phenomenon raises the interest on investigating about its behaviour under the usual working conditions of a cathode in SOFC.

The aim of this study is to correlate the thermal evolution of the crystal structure of highly oxygenated $La_2Ni_{0.6}Cu_{0.4}O_{4+\delta}$ with the observed changes in the electrical behaviour in the temperature range between 25 and 900 °C. The stability of the electrical conductivity and the thermal expansion of this material will also be analyzed.

2. Experimental

Polycrystalline $La_2Ni_{0.6}Cu_{0.4}O_{4+\delta}$ powder was synthesized via a nitrate-citrate route. Stoichiometric amounts of analytical grade La_2O_3, $Ni(NO_3)_2{\cdot}6H_2O$ and CuO (Panreac) were dissolved in 8 M HNO_3 (Merck). Citric acid was then added to the mixture in a molar ratio 3.3:1 with regard to $La_2Ni_{0.6}Cu_{0.4}O_{4+\delta}$. The resulting product was dehydrated before being calcined at 600 °C for 30 min. Finally, it was fired in air at 950 °C for 8 h and slowly cooled down to room temperature. Subsequent heat treatment under high oxygen pressure was performed at 350 °C and 200 bar of oxygen during 12 h in a VAS furnace. Raw and O_2-treated samples were characterized by X-ray diffraction (XRD) for phase identification and to assess phase purity. XRD analysis was performed in a Philips "X Pert-MPD" diffractometer using Cu Kα radiation (λ = 1.5406 Å). The diffraction patterns were recorded in the 2θ range 20–80 with steps of 0.04°. The cationic ratios were determined by inductively coupled plasma-atomic emission spectroscopy (ICP-AES) using a Jobin Yvon equipment.

The oxygen content (δ) of the sample at RT was determined by thermogravimetric analysis and Rietveld refinement from the neutron powder diffraction (NPD) measurements. The thermogravimetric analysis was performed by heating the sample up to 900 °C in a H_2/N_2 (5:95) flow using a Mettler-Toledo equipment. The thermal evolution of the oxygen content of O_2-treated $La_2Ni_{0.6}Cu_{0.4}O_{4+\delta}$ in air was also studied. In addition, the thermal behaviour of this material was analysed by differential scanning calorimetry (DSC) and thermogravimetric analysis in air. For this purpose, the sample (100 mg) was placed in an aluminium can and cycled several times in air in a SEIKO DSC 220U equipment in the 25–600 °C temperature range.

The *in situ* neutron diffraction measurements were performed in the high flux reactor at the Institute Laue-Langevin in Grenoble, France. The high resolution D2B diffractometer was used with a wavelength λ = 1.594 Å selected from a Ge monochromator. The diffraction pattern covered the range 5–165° in 2θ. Measurements were carried out in air in each interval of 100 °C from 25 to 900 °C. For this purpose, the sample was contained in a quartz tube open to the ambient atmosphere, placed in the isothermal zone of a furnace with a vanadium resistor operating under vacuum ($P_{O_2} \approx 10^{-6}$ Torr).

Rietvelt refinements of the crystal structure were performed using the FULLPROF program [19]. The line shape of the diffraction peaks was generated by a pseudo-Voigt function. The strong background arising from the quartz container was esti-

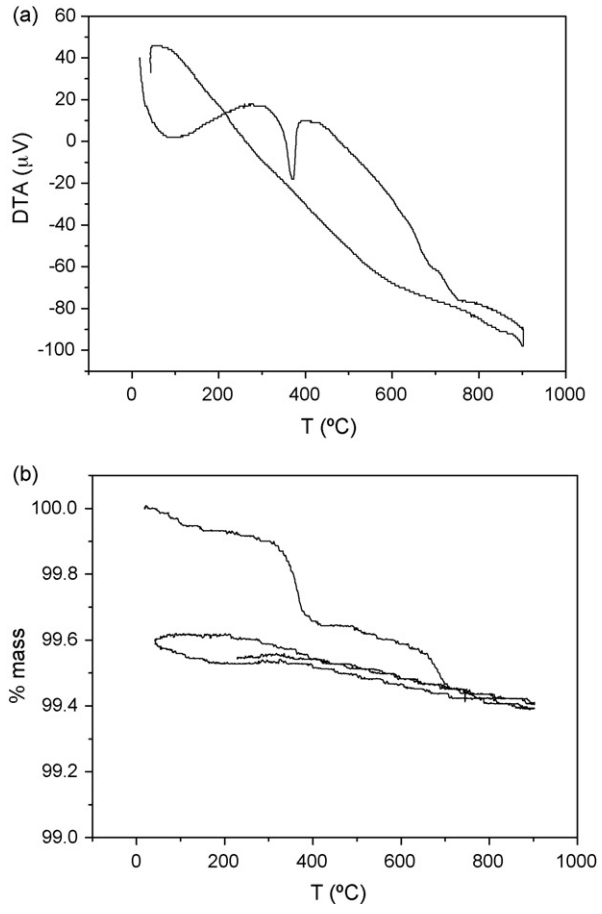

Fig. 1. Thermal analysis for $La_2Ni_{0.6}Cu_{0.4}O_{4.16}$: (a) DTA curves under static air in the *T* range 25–900 °C and (b) thermogravimetric curves under static air cycled from 25 to 900 °C.

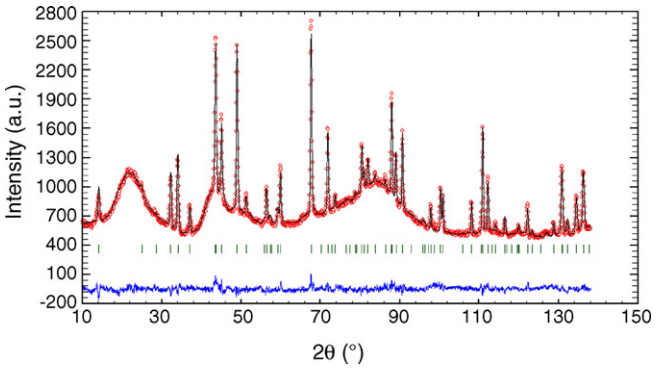

Fig. 2. Observed (circles) and calculated (full curve) neutron diffraction profiles at 25 °C for $La_2Ni_{0.6}Cu_{0.4}O_{4.16}$ using a single phase *F*4/*mmm* model.

mated by interpolation between selected points in regions devoid of Bragg reflections. In the final run the following parameters were refined: zero point, half width, pseudo-Voigt and asymmetry parameters for the peak shape, scale factor and unit cell parameters, positional parameters, occupancy factors for oxygen atoms and isotropic thermal factors. The scattering lengths for La, Ni, Cu and O are, respectively, 8.24, 10.30, 7.718 and 5.803 fm.

Dense compounds are required for the measurements of thermal expansion coefficient and electrical conductivity. The prepared powders were pressed into pellets (10 mm in diameter and 1.4 mm think) using polyethylene glycol as a binder and 3 tonnes of uniaxial pressure during 5 min. The sintering behaviour of green compacts and thermal expansion of dense ceramics were studied using a Linseis L75/1550C dilatometer with a heating rate of 5 °C min^{-1}. The optimal sintering temperature and dwelling time obtained was 1250 °C for 4 h.

Total conductivity measurements were carried out from 25 to 900 °C by the four probe method in air on dense ceramics of the material under study. For this purpose the as-prepared powder was pressed into pellets (10 mm in diameter and 1.4 mm thick) using polyethylene glycol as a binder. Finally, the dense pellet subsequently underwent a thermal treatment under high oxygen pressure (350 °C, 200 bar). For the conductivity measurements, the dense ceramic was placed onto an alumina support and four platinum wires contacts were pressed onto the surface of the sample using a spring-loaded alumina tube. Current load of 100 mA was applied by a potentiostat/galvanostat (EG&G Model 263) and the potential drop recorded by a Fluke 179 True RMS Multimeter.

3. Results and discussion

X-ray powder diffraction data are characteristic of well-crystallized K_2NiF_4 powders for both as-prepared and

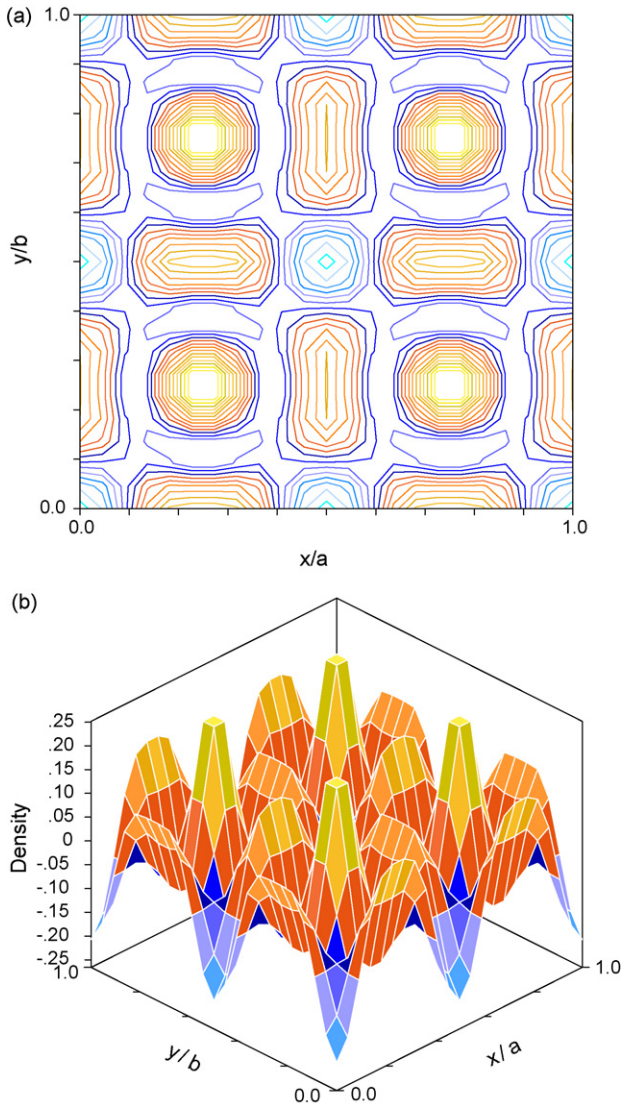

Fig. 3. Localization of the interstitial oxygen atoms (O4) by Fourie analysis of difference.

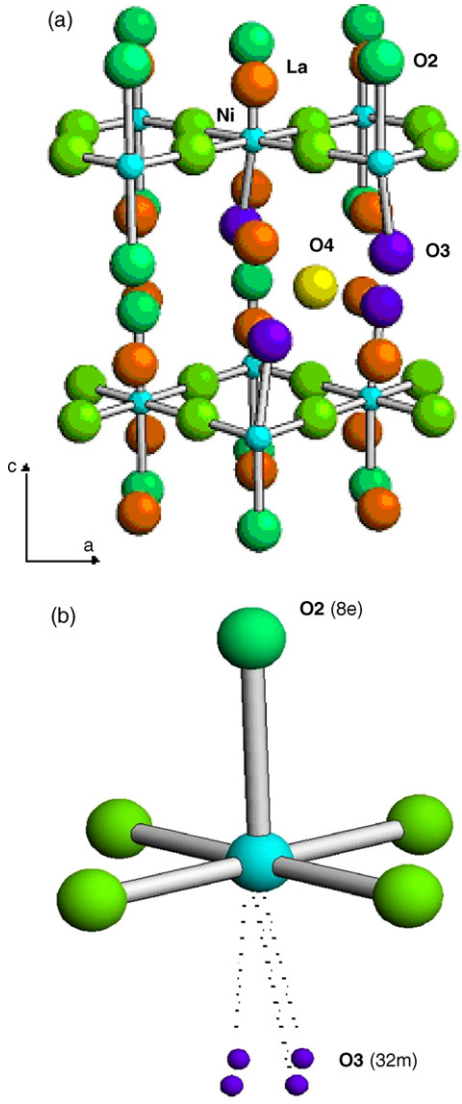

Fig. 4. (a) Crystal structure of $La_2Ni_{0.6}Cu_{0.4}O_{4.16}$: O1 are the equatorial oxygen atoms of the NiO_6 octahedra whereas O2 and O3 are the axial ones and (b) multiplicity of the novel axial O3 position.

O_2-treated (350 °C/200 bar) samples. ICP-AES data confirmed the cationic ratio to be as expected, excluding the presence of lanthanum vacancies.

3.1. Thermal analysis

Thermogravimetric analysis curves in H_2/N_2 flow evidence an increase of the excess of oxygen (δ) with the O_2-treatment from 0.07(2) to 0.16(2) moles of oxygen per formula unit of $La_2Ni_{0.6}Cu_{0.4}O_{4+\delta}$. Hereafter, the O_2-treated (350/200 bar O_2) sample will be labelled as $La_2Ni_{0.6}Cu_{0.4}O_{4.16}$.

The DTA curves under static air of $La_2Ni_{0.6}Cu_{0.4}O_{4.16}$, carried out from 25 to 900 °C are showed in Fig. 1a. In the heating stage there is a peak centred at 380 °C; this peak was identified as an oxygen release process, in agreement with the weight loss observed in the TG curves (Fig. 1b). In the cooling stage no peaks were observed, suggesting that the process is irreversible.

The thermogravimetric curves shown in Fig. 1b were carried out in air with several heating–cooling cycles from 25 to 900 °C. An irreversible loss of 0.09 mol of oxygen per formula unit was observed in the first cycle. The subsequent heating–cooling cycles reveal small reversible losses.

3.2. Neutron diffraction results

The thermal evolution of the crystal structure of the O_2-treated sample was studied by NPD; the data were collected *in situ* in a furnace in the temperature range 25–900 °C each 100 °C.

Owing to our previous study on the crystal structure of $La_2Ni_{0.6}Cu_{0.4}O_{4+\delta}$ [11], in a first trial, the crystal structure of $La_2Ni_{0.6}Cu_{0.4}O_{4.16}$, was Rietveld-refined at room temperature (RT) as an orthorhombic single phase defined in the *Bmab* space group with $R_{Bragg} = 11.7\%$. However, subsequent refinement in the orthorhombic *Fmmm* and in the tetragonal *F4/mmm* space groups leads to $R_{Bragg}(\%) = 9.35$ and $R_{Bragg}(\%) = 6.22$, respectively. Therefore, the tetragonal *F4/mmm* space group was chosen for the refinement. The better agreement with the tetragonal *F4/mmm* space group can be explain due to the higher oxygen content that lead to the relaxation of the lattice stress between the La_2O_2 and the NiO_2 layers.

In spite of the irregular background resulting from the quartz container, we have achieved a good agreement between observed and calculated profiles (Fig. 2). The model proposed by Jorgensen et al. was selected for the RT refinement [15]. In

Table 1a
Structural parameters after the Rietveld refinement from NPD data for $La_2Ni_{0.6}Cu_{0.4}O_{4.16}$ at 25, 100, 200, 300 and 400 °C

T (°C)	25	100	200	300	400
$a = b$ (Å)	5.43156(8)	5.43328(8)	5.43891(8)	5.44525(9)	5.45242(9)
c (Å)	12.8847(3)	12.8924(3)	12.9134(3)	12.9327(3)	12.9423(3)
V (Å^3)	380.12(1)	380.59(1)	382.00(1)	383.46(1)	384.768(1)
La					
z	0.3603(2)	0.3602(2)	0.3606(2)	0.3604(2)	0.3612(2)
B (Å^2)	1.179(4)	1.230(4)	1.35(4)	1.46(4)	1.50(4)
n	1	1	1	1	1
Ni(Cu)					
B (Å^2)	0.98(4)	0.93(4)	1.11(5)	1.36(5)	1.25(5)
N (Cu)	0.2	0.2	0.2	0.2	0.2
O1					
B (Å^2)	1.24(5)	1.41(5)	1.55(6)	1.56(5)	1.64(6)
n	1	1	1	1	1
O2					
z	0.1756(6)	0.1760(6)	0.1762(7)	0.1784(9)	0.177(1)
B (Å^2)	1.08(8)	1.49(9)	1.59(9)	1.9(1)	2.2(1)
n	0.6	0.6	0.6	0.6	0.6
O3					
$x = y$	−0.066(1)	−0.062(2)	−0.064(2)	−0.063(2)	−0.55(2)
z	0.188(1)	0.185(2)	0.184(2)	0.179(2)	0.183(2)
B (Å^2)	1.08(8)	1.49(9)	1.59(9)	1.9(1)	2.2(1)
n	0.4	0.4	0.4	0.4	0.4
O4					
z	0.25	0.25	0.25	0.25	0.25
B (Å^2)	1.0	1.0	1.0	1.0	1.0
n	0.080(5)	0.100(5)	0.087(5)	0.078(5)	0.068(5)
χ^2	2.64	2.40	2.59	2.67	2.86
R_p (%)	2.47	2.38	2.51	2.49	2.55
R_{wp} (%)	3.07	3.01	3.20	3.18	3.29
R_{exp} (%)	2.09	2.09	2.09	2.09	2.11
R_{Bragg}	10.6	8.14	10.7	10.9	9.77

Space group *F4/mmm*, La and O2 at 8e (0, 0, z) sites, Ni and Cu at 4a (0, 0, 0), O1 at 8c (1/4, 1/4, 0), O3 at 32m (x, y, z) and O4 at 16e (1/4, 1/4, z) positions.

Table 1b
Structural parameters after the Rietveld refinement from NPD data for $La_2Ni_{0.6}Cu_{0.4}O_{4.16}$ at 500, 600, 700, 800 and 900 °C

T (°C)	500	600	700	800	900
$a = b$ (Å)	5.45959(9)	5.4674(1)	5.4752(1)	5.4832(1)	5.4913(1)
c (Å)	12.9587(3)	12.9756(4)	12.9922(4)	13.0096(4)	13.0290(4)
V (Å^3)	386.26(1)	387.87(2)	389.49(2)	391.14(2)	392.88(2)
La					
z	0.3614(2)	0.3614(2)	0.3606(2)	0.3618(2)	0.3617(2)
B (Å^2)	1.77(4)	1.94(5)	2.06(6)	2.28(6)	2.56(6)
n	1	1	1	1	1
Ni (Cu)					
B (Å^2)	1.26(5)	1.63(6)	1.79(6)	1.98(7)	2.06(7)
N (Cu)	0.2	0.2	0.2	0.2	0.2
O1					
B (Å^2)	1.81(6)	2.13(7)	2.17(7)	2.52(8)	2.85(8)
n	1	1	1	1	
O2					
z	0.179(1)	0.1778(9)	0.179(1)	0.1776(9)	0.178(1)
B (Å^2)	2.5(1)	2.3(1)	2.5(2)	2.4(1)	2.7(2)
n	0.6	0.6	0.6	0.6	0.6
O3					
$x = y$	−0.057(2)	−0.061(2)	−0.058(2)	−0.069(2)	−0.064(2)
z	0.184(2)	0.187(2)	0.186(2)	0.189(2)	0.184(2)
B (Å^2)	2.5(1)	2.3(1)	2.5(2)	2.4(1)	2.7(2)
n	0.4	0.4	0.4	0.4	0.4
O4					
z	0.25	0.25	0.25	0.25	0.25
B (Å^2)	1.0	1.0	1.0	1.0	1.0
n	0.068(5)	0.070(5)	0.060(6)	0.051(6)	0.058(6)
χ^2	2.44	2.71	2.75	2.65	2.59
R_p (%)	2.45	2.51	2.52	2.53	2.49
R_{wp} (%)	3.10	3.25	3.21	3.26	3.15
R_{exp} (%)	2.11	2.11	2.11	2.11	2.10
R_{Bragg}	10.4	2.37	13.5	14.5	12.6

Space group *F*4/*mmm*, La and O2 at 8e (0, 0, *z*) sites, Ni and Cu at 4a (0, 0, 0), O1 at 8c (1/4, 1/4, 0), O3 at 32m (*x*, *y*, *z*) and O4 at 16e (1/4, 1/4/, *z*) positions.

*F*4/*mmm*, La and O2 atoms are located at 8e (0, 0, *z*) sites, Ni at 4a (0, 0, 0), O1 at 8c (1/4, 1/4, 0), O3 at 32m (*x*, *y*, *z*) and the interstitial O4 atoms at 16e (1/4, 1/4, *z*) positions. The O4 site corresponds to interstitial oxygen atoms whose real position was determined to be effectively at (1/4, 1/4, 1/4) by differential Fourier analysis (Fig. 3). The insertion of these additional oxygen atoms into the lattice causes a displacement of the axial O2 oxygen from its normal location to a new axial O3 position leading to a novel split position, as illustrated in Fig. 4. Therein, the complementary occupancies of the axial O2 positions and the displaced axial O3 oxygens were constrained to 1.00, and the isothermal factors were also constrained.

Subsequent structural refinement from NPD data collected at $T \geq 100$ °C shows no structural transition along the temperature

Table 2a
Main interatomic distances (Å) for $La_2Ni_{0.6}Cu_{0.4}O_{4.16}$ determined from NPD data at 25, 100, 200, 300 and 400 °C

Bond/T (°C)	25	100	200	300	400
La–O1 × 4	2.632(2)	2.634(2)	2.634(2)	2.639(2)	2.635(2)
La–O2	2.380(8)	2.375(9)	2.38 (1)	2.35(1)	2.38(2)
La–O2 × 4	2.755(1)	2.756(2)	2.761(2)	2.768(2)	2.771(3)
La–O3	2.29(2)	2.31(2)	2.33(2)	2.39(3)	2.34(3)
La–O3	2.460(9)	2.474(9)	2.47(1)	2.46(1)	2.51(1)
La–O4	2.389(1)	2.390(1)	2.395(2)	2.397(2)	2.406(2)
Ni(Cu)–O1 × 4	1.9203(0)	1.9210(0)	1.9229(0)	1.9252(0)	1.9277(0)
Ni(Cu)–O2 × 2	2.263(7)	2.269(8)	2.276(9)	2.31(1)	2.29(1)
Ni(Cu)–O3	2.46(2)	2.43(2)	2.43(2)	2.37(3)	2.411(2)
O4–O3 × 4	2.562(9)	2.538(1)	2.56(1)	2.58(1)	2.51(2)
O4–O3 × 4	1.63(1)	1.67(1)	1.66(1)	1.71(2)	1.73(2)
O4–O3 × 8	2.15(1)	2.15(1)	2.16(1)	2.19(1)	2.15(2)

Table 2b
Main interatomic distances (Å) for $La_2Ni_{0.6}Cu_{0.4}O_{4.16}$ determined from NPD data at 500, 600, 700, 800 and 900 °C

Bond/*T* (°C)	500	600	700	800	900
La–O1 × 4	2.636(2)	2.640(2)	2.651(2)	2.644(2)	2.649(2)
La–O2	2.37(2)	2.38(1)	2.36(2)	2.40(12)	2.40(2)
La–O2 × 4	2.779(3)	2.781(2)	2.785(3)	2.789(2)	2.794(3)
La–O3	2.34(3)	2.31(3)	2.31(3)	2.31(3)	2.36(3)
La–O3	2.51(1)	2.51(1)	2.52(2)	2.48(1)	2.49(1)
La–O4	2.410(2)	2.414(2)	2.411(2)	2.424(2)	2.427(2)
Ni(Cu)–O1 × 4	1.9303(0)	1.9330(0)	1.9358(0)	1.9386(0)	1.9415(0)
Ni(Cu)–O2 × 2	2.32(2)	2.31(1)	2.32(2)	2.31(1)	2.32(2)
Ni(Cu)-O3	2.42(3)	2.48(3)	2.46(3)	2.51(2)	2.47(3)
O4–O3 × 4	2.52(2)	2.54(1)	2.53(2)	2.60(1)	2.59(2)
O4–O3 × 4	1.72(2)	1.67(2)	1.70(2)	1.62(2)	1.67(2)
O4–O3 × 8	2.16(2)	2.15(2)	2.15(2)	2.16(1)	2.18(2)

range under study (25–900 °C). Thus, the data collected between 25 and 900 °C were successfully refined in the *F*4/*mmm* space group. Tables 1a and 1b summarises the results obtained from these refinements. This behaviour is in agreement with the DSC results previously observed. As shown in Fig. 5, the unit-cell parameter *a* increases with the temperature whereas *c* presents an anomalous growth between 300 and 400 °C. This can be understood as a cell contraction along the *c* direction at this temperature superpose to the thermal expansion of the cell at this temperature range.

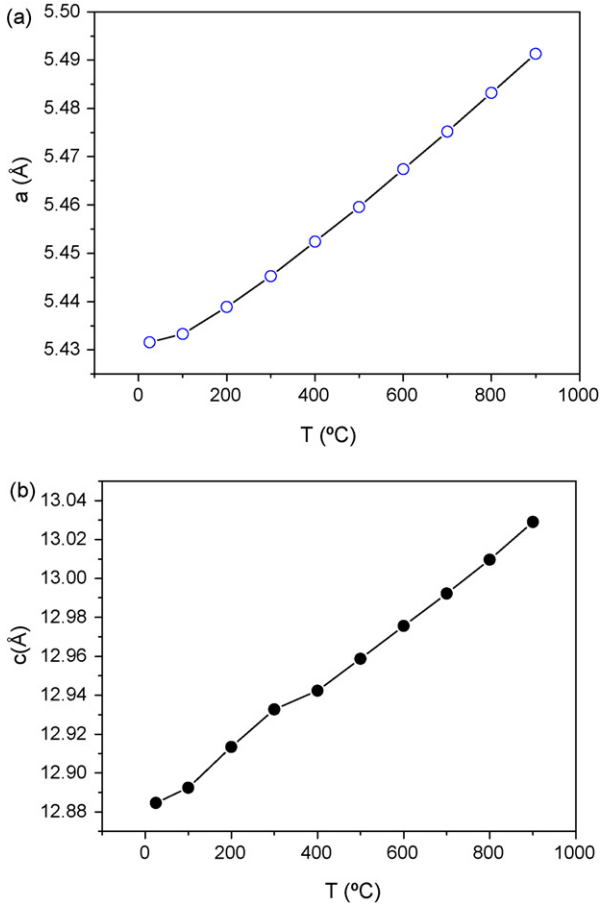

Fig. 5. Thermal evolution of lattice parameters of $La_2Ni_{0.6}Cu_{0.4}O_{4.16}$ from RT to 700 °C: (a) *a* and *b* parameters and (b) *c* parameter.

Tables 2a and 2b includes the main bonding distances for $La_2Ni_{0.6}Cu_{0.4}O_{4.16}$. La–O1 bond lengths are not highly influenced by temperature, exhibiting an average increase of 0.017 Å from RT to 900 °C. There are two types of La–O2 bond lengths (along the *c*-axis); the bigger one is larger than the corresponding sum of the ionic radii of O^{2-} and eight-coordinated La^{3+} ions (2.56 Å), the second one being smaller. The shortest La–O2 distance is responsible of the cohesion between the perovskite and the rock-salt layer.

The temperature dependence of the Ni–O interatomic distances is represented in Fig. 6. Equatorial Ni–O1 bond lengths linearly increase with temperature, scaling with the concomitant increment of *a* unit-cell parameter. Conversely, axial Ni–O2 bond lengths increase with temperature but display a contraction at 400 °C which can be associated with the axial compression observed for the *c* unit-cell parameter.

3.3. Thermal expansion coefficients

Aiming to determine the mechanical compatibility of our material with the other cell components, thermal expansion measurement of the dense ceramic was carried out in air in the temperature range 25–1000 °C (Fig. 7). The thermal expansion coefficients obtained from the slope of the line at different temperatures is summarized in Table 3. The values obtained are very close to that of the usual SOFC electrolytes.

3.4. Transport properties

The total electrical conductivity (σ) of sintered ceramics was investigated in the temperature range of 25–900 °C. Fig. 8 shows a change in the conduction regime from semiconductor-like below 400 °C, exhibiting a maximum conductivity of 110 S cm^{-1}, followed by a high-temperature regime charac-

Table 3
Thermal expansion coefficients (TEC) for $La_2Ni_{0.6}Cu_{0.4}O_{4.16}$ at 600, 700 and 800 °C

$TEC_{50–1000\,°C}$ ($10^{-6}\,K^{-1}$)	$TEC_{50–800\,°C}$ ($10^{-6}\,K^{-1}$)	$TEC_{50–600\,°C}$ ($10^{-6}\,K^{-1}$)
13.02	12.93	12.60

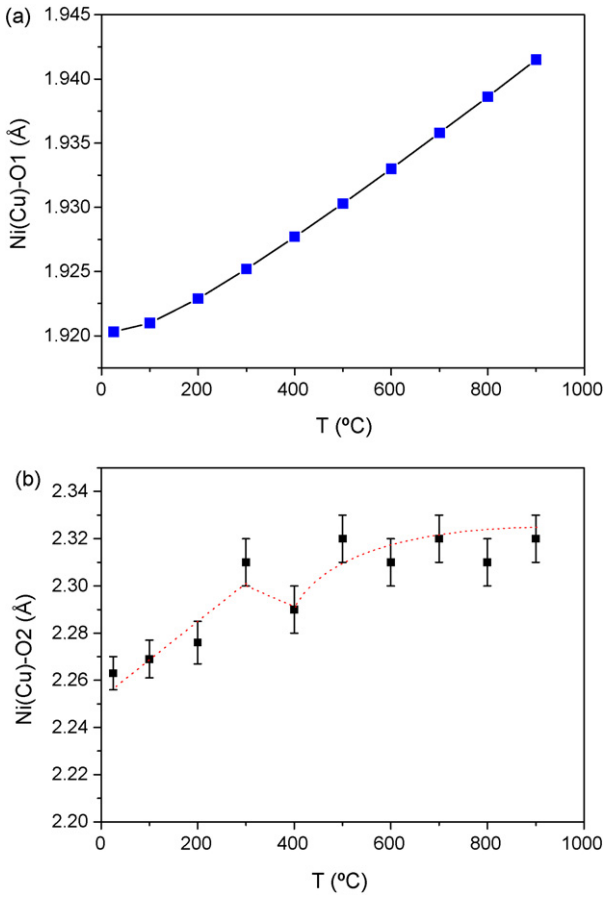

Fig. 6. Variation of Ni–O bond lengths for $La_2Ni_{0.6}Cu_{0.4}O_{4,16}$ as a function of temperature: (a) Ni-O1 (the error bars are smaller that the symbol size) and (b) Ni–O2.

terized by a negative slope, which could be labelled as metal behaviour. We can correlate this behaviour with the observed contraction in the axial Ni–O2 bond lengths at 400 °C. In this material, the electronic conductivity is due to electron hopping along Ni–O–Ni linkage, in such a way that it is sensitive to the contraction of the Ni–O2 bonds along the axial direction. This behaviour is reminiscent to that observed in $RNiO_3$ perovskites, where a metal–insulator transition is observed as a function

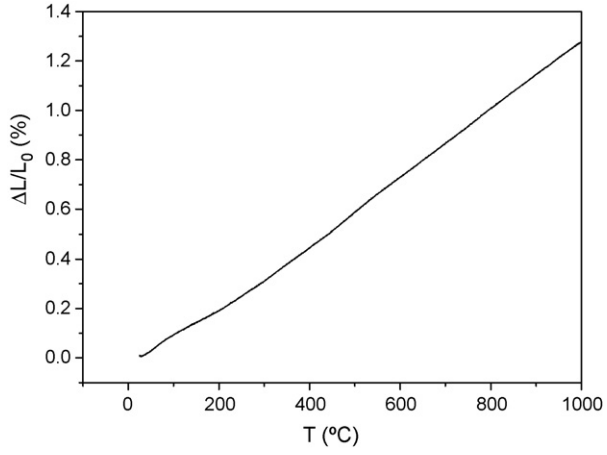

Fig. 7. Thermal expansion of $La_2Ni_{0.6}Cu_{0.4}O_{4.16}$.

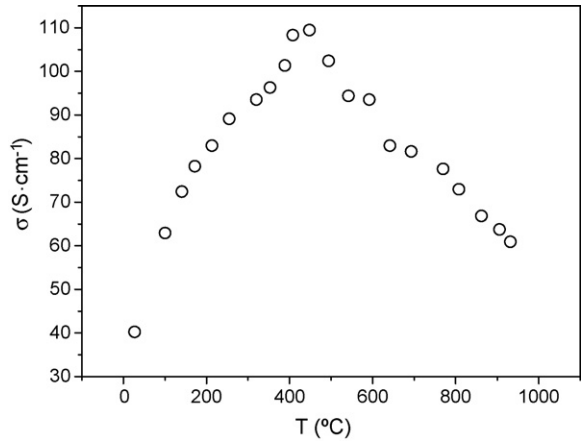

Fig. 8. Electrical conductivity for $La_2Ni_{0.6}Cu_{0.4}O_{4.16}$ at different temperatures.

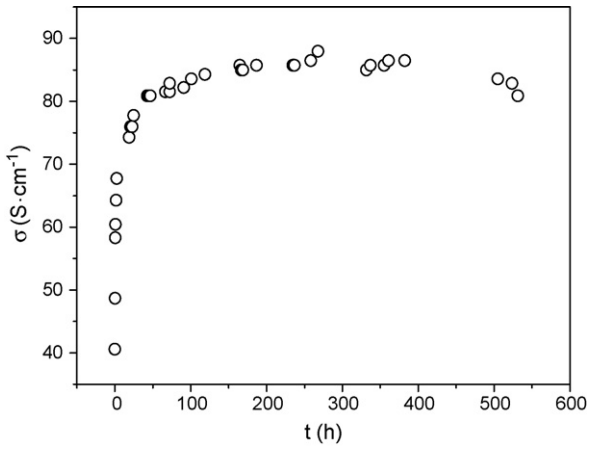

Fig. 9. Thermal stability of the conductivity at 750 °C.

of temperature (T_{MI}) and the size of the rare earth. The conductivity displays a metallic behaviour in the high temperature region and an insulating (semiconducting) behaviour in the low temperature interval, exhibiting a maximum conductivity at T_{MI}. An *in situ* structural study by NPD for $RNiO_3$ perovskites also shows an abrupt structural change coincident with the metal insulator transition [20], in the sense that an abrupt contraction of the average Ni–O distances is observed upon metallization, at T_{MI}. We report a parallel effect, although weaker, in the strongly related $La_2NiO_{4+\delta}$ phases, with K_2NiF_4 structure, where a metal (high T)–insulator (low T) transition can be microscopically correlated with a contraction of Ni–O bonds upon metallization.

We have also performed an experiment of the electrical conductivity at 750 °C during 580 h. Fig. 9 evidence that the sample conserve its conductivity value constant to 87 S cm^{-1} along 580 h at this temperature.

4. Conclusions

The synthesis of O_2-treated $La_2Ni_{0.6}Cu_{0.4}O_{4+\delta}$ (350 °C/200 bar) leads to a highly oxygenated sample with composition $La_2Ni_{0.6}Cu_{0.4}O_{4.16}$. There are no structural transitions along the temperature range studied (25–900 °C). Therefore, the

compound has been defined in the tetragonal *F*4/*mmm* space group at all temperatures.

We can establish a correlation between the axial Ni–O2 bond length and the electrical conductivity behaviour. The observed contraction of the Ni–O2 distance at 400 °C seems to be concomitant maximum value of conductivity (110 S cm^{-1}) at around 400 °C. We can conclude that the electrical conductivity in $La_2Ni_{0.6}Cu_{0.4}O_{4.16}$ has a strong anisotropic component and it is highly affected by the shrinkage in the perovskite layer along the *c* direction. We have also performed a durability experiment at 750 °C for 560 h obtaining a very stable value for the electrical conductivity of 87 S cm^{-1}. The thermal expansion coefficient was 13–12.6 × 10^{-6} K^{-1} very closet to that of the usual SOFC electrolytes at these temperatures (600–1000 °C).

Acknowledgements

We thank the financial support of the Spanish Ministerio de Educación y Ciencia to the MAT2004-0479 project and of Madrid Community to the ENERCAM-CM S-0505/ENE/0304 project. A.A. also wants to acknowledge CIEMAT for a grant. We thank the Institute Laue Langevin, Grenoble, France, for making all facilities available.

References

[1] J. Fleig, J. Maier, J. Eur. Ceram. Soc. 24 (2004) 1343–1347.
[2] H.J.M. Bounwmeester, S. McIntosch, Proceedings of the 26th Risoe International Symposium on Solid State Electrochemistry, Denmark, 2005, pp. 1–14.
[3] V.V. Kharton, A.P. Viskup, A.V. Kovalvsky, E.N. Naumovich, F.M.B. Marques, Solid State Ionics 143 (2001) 1174–1178.
[4] Y. Wang, H. Nie, S. Wang, T. Wen, U. Guth, V. Valshook, Mater. Lett. 60 (2006) 26–37.
[5] V.V. Kharton, A.A. Yaremchenco, A.L. Shaula, M.V. Patrekeev, E.N. Naumovich, D.I. Logvinovich, J.R. Frade, F.M.B. Marques, J. Solid State Chem. 177 (2004) 26–37.
[6] E.N. Naumovich, M.V. Patrakeev, V.V. Kharton, A.A. Yaremchenko, D.I. Logvinovich, F.M.B. Marques, Solid State Sci. 7 (2005) 1353–1362.
[7] V.V. Kharton, A.A. Yaremchenko, E.N. Naumovich, J. Solid State Electrochem. 3 (1999) 303–326.
[8] L. Minervini, R.W. Grimes, J.A. Kilner, K.E. Sickafus, J.-C. Grenier, Ph. Stevens, J. Mater. Chem. 10 (2000) 2349–2354.
[9] J.M. Bassat, P. Odier, A. Villesuzane, C. Marin, M. Pouchard, Solid State Ionics 167 (2005) 52–56.
[10] E. Boehm, J.M. Bassat, P. Dordor, F. Mauvy, J.-C. Grenier, Ph. Stevens, Solid State Ionics 176 (2005) 2717–2725.
[11] A. Aguadero, M. Perez, J.A. Alonso, L. Daza, J. Power Sources 151 (2005) 52–56.
[12] D.E. Rice, D.J. Buttrey, J. Solid State Chem. 105 (1993) 197–210.
[13] A. Metha, P.J. Heaney, Phys. Rev. B 49 (1994) 563–571.
[14] W. Paulus, A. Cousson, G. Dhalenne, J. Berthon, A. Revcoleuschi, S. Hosoya, W. Treutmann, G. Heger, R.L.E. Toquin, Solid State Sci. 4 (2002) 565–573.
[15] J.D. Jorgensen, B. Dabrowski, S. Pei, D.R. Richards, D.G. Hinks, Phys. Rev. B 40 (1989) 2187–2199.
[16] M.T. Fernández-Díaz, J.L. Martínez, J. Rodríguez-Carvajal, Solid State Ionics 63 (1993) 902–906.
[17] S.J. Skinner, Solid State Sci. 5 (2003) 419–426.
[18] A. Aguadero, J.A. Alonso, M.J. Martínez-Lope, M.T. Fernández-Díaz, M.J. Escudero, L. Daza, J. Mater. Chem. 16 (2006) 3402–3408.
[19] J. Rodríguez-Carvajal, Physica B 192 (1993) 55–69.
[20] J.L. García-Muñoz, J. Rodríguez-Carvajal, P. Lacorre, J.B. Torrance, Phys. Rev. B 46 (1992) 4414–4420.